LARGE EDDY SIMULATIONS OF PARTICLE DEPOSITION IN A TURBULENT SQUARE DUCT FLOW

Chad M. Winkler, Sarma L. Rani, and S. Pratap Vanka
Department of Mechanical and Industrial Engineering, University of Illinois at Urbana-Champaign,
1206 W. Green St., Urbana, Illinois 61801 USA
cmwinkle@uiuc.edu, rani@uiuc.edu, s-vanka@uiuc.edu

ABSTRACT

The deposition of heavy solid particles in a downward, fully developed turbulent square duct flow at $Re_\tau = 360$, based on average friction velocity and duct width, is studied using large eddy simulations. The continuous and the dispersed phases are treated using the Eulerian and Lagrangian approaches, respectively. A finite volume based second-order accurate fractional step scheme is used to integrate the incompressible form of the unsteady, three-dimensional Navier-Stokes equations on an 80×80×128 grid. A dynamic subgrid kinetic energy model is used to account for the subgrid scales. The particle equation of motion includes drag, lift, and gravity forces and is integrated using the fourth-order accurate Runge-Kutta method. Table 1 lists the details of the particle properties. Three approaches are used in this work. First, simulations are carried out assuming that the particle-particle interactions are negligible and that the particles do not modify the fluid phase momentum (one-way coupling). Second, simulations are carried out for representative cases with the inclusion of particle-particle collisions as well as particle feedback effects on the fluid phase (four-way coupling). Third, collisions are neglected but the particle feedback effect is retained (two-way coupling) for a select case to determine if the observed trends are due to collisions or due to two-way coupling.

Variation in the probability distribution function (PDF) of the deposition location with particle Stokes number is presented. The average streamwise and wall-normal deposition velocities are also presented. Collisions are seen to increase the deposition rates.

INTRODUCTION

Particle deposition is influenced by the turbulent flow structures which are known to cause preferential concentration of particles (Squires and Eaton, 1991; Fessler et al., 1994). There have been a number of previous studies on particle deposition in channels and pipes (Wang and Squires, 1996). However, relatively few studies on flows with only one homogeneous direction, such as a square duct, have been performed. For single-phase flow, one of the first LES studies of secondary flows in a square duct was performed by Madabhushi and Vanka (1991) using the Smagorinsky model and a 65×65×32 grid. They studied flow at $Re_\tau = 360$ based on duct width and average friction velocity. LES was shown to successfully predict the turbulence driven secondary flows. Other studies of secondary flows include those by Kajishima and Miyake (1992), and Gavrilakis (1992). In the present study, particle deposition in a fully developed turbulent square duct flow is investigated

Particle deposition in a channel flow was studied with LES by Wang and Squires (1996). The maximum particle concentration was found to be near the wall. When the LES results were compared with those of DNS, the particles with the largest relaxation times were found to compare the best. This is because larger particles are less likely to be influenced by the small scales which are not accurately represented by LES. It was also found that the lift force increases particle deposition.

Zhang and Ahmadi (2000) examined aerosol particle transport and deposition in channels. For horizontal ducts, they found that gravity increases deposition by sedimentation on the lower wall. For vertical ducts, when gravity was in the flow direction, deposition rates were higher since the lift force will now act towards the walls.

Uijttewaal and Oliemans (1996) examined particle dispersion and deposition in vertical pipes of circular cross-section. They found that the deposition coefficient scales with the turbulence integral time scale. The wall impact velocity was seen to peak around $\tau_p^+ = 200$. To more accurately represent the dispersion of small particles, they also suggest taking into account the effects of the subgrid turbulence on the particle motion.

Despite the relatively large number of works on particle deposition in turbulent flows, there is a lack of information on this phenomenon in complex geometries. Mean secondary flows, show in Fig. 1, will add complexity to the particle deposition. In the present study, particle deposition in a fully developed turbulent square duct flow is investigated.

NUMERICAL METHOD

The incompressible three-dimensional, unsteady Navier-Stokes equations are solved using a second-order accurate finite volume method on a collocated grid with central differencing of the spatial derivatives. The friction Reynolds number based on mean friction velocity, $u_\tau = \left(\bar{\tau}_w/\rho_f\right)^{1/2}$, and duct width, δ, is $Re_\tau = 360$, where $\bar{\tau}_w$ and ρ_f are the mean wall shear stress and the fluid density, respectively. Diffusion and the convective terms are discretized with the Crank-Nicholson and the second-order accurate Adams-Bashforth schemes, respectively. An algebraic multigrid solver was used to solve the pressure Poisson equation resulting from the fractional step method. The square duct dimensions in the x, y, and z directions are $\delta \times \delta \times 2\pi\delta$ and the grid consisted of $80 \times 80 \times 128$ Cartesian cells. The unresolved scales are modeled with the dynamic subgrid kinetic energy model developed by Kim and Menon (1997). The particle equation of motion includes drag, lift in the two wall directions (x and y) and gravity in the streamwise direction (z). Several particle response times and volume fractions are studied to identify statistical trends of the effects of secondary flows on particle deposition. One-way, two-way, and four-way coupling effects are separately examined. A new approach for accounting collisions between particles, which is more accurate than the purely retroactive method and is computationally less intensive than the proactive method, has been developed and used in the current work.

Particle Motion

Subgrid fluctuations, $\sqrt{2\,k_{sgs}/3}$, are scaled by a Gaussian distributed random number and isotropically added to the fluid velocity at the particle position to more accurately represent the instantaneous velocity. Particles are assumed to deposit when they are within one radius from a wall. The particles, initially, are randomly positioned in the domain with initial velocities equal to the local fluid velocity. Since it is only by chance that a particle is located at a fluid grid point, second order Lagrange polynomials were used to interpolate the fluid quantities to a particle position. This involved interpolating values of fluid quantities (such as u, v, w and k_{sgs}) at 27 locations surrounding the particle.

Particle Collisions

An approach that is more accurate than the purely retroactive method and is computationally less intensive than the proactive method has been developed and used in the current work. The current method is briefly described below.

The flow domain is first partitioned into sections in which collisions will be considered. In this work, $16 \times 16 \times 16$ uniform partitions are used. It is assumed that the particles have constant velocities during a time step. In a given partition, all collision pairs are first identified using a method similar to Chen et al. (1998). Next, the pairs are ordered in the ascending order of their time for collision. The first collision in the ordered list (say, between particles p and q) for the partition is carried out by advancing the particles p and q to the point of impact by using the velocities at the n^{th} time step. Perfectly elastic collisions are assumed to compute post-collision particle velocities. The collision list is then modified such that any future collision that contains particles p and q is not allowed to occur in the same time step. Subsequently, the pair next in the list to p and q is made to collide and is then removed from future collisions during the current time step. This process is repeated until there are no more particles left in the collision list. The inclusion of this collision algorithm required approximately three times more CPU time for a given simulation compared to that without collisions. Full details of the algorithm will be presented in a forthcoming technical note.

RESULTS

The mean fluid statistics are averaged in time for more than 60 dimensionless time units. Further, the deposition statistics are averaged in time (34 time units for the $\tau_p^+ = 0.072$ particles and 8 time units for the $\tau_p^+ = 256.32$ particles), in the homogeneous streamwise direction, and over the four duct walls (due to a 90° rotation symmetry about the duct axis in the cross-sectional plane). One-way coupling results will be presented first, followed by a discussion of the effects of two-way and four-way coupling.

The unladen fluid flow results were compared to the DNS data of Madabhushi (1993), and to the LES data of Madabhushi and Vanka (1991), who studied flow at $Re_\tau = 260$ and 360, respectively. Good agreement is seen in Fig. 2 where the mean streamwise velocity at the wall bisector from the current simulation is compared to that from the above two studies.

One-way coupling

Wall-Normal Deposition Velocity. The deposition velocities in the wall-normal and the streamwise directions are of interest in studying the erosion of the duct walls. In a channel or a pipe flow, the deposition velocity is a constant over the wall due to the spatial averaging in the two homogeneous directions parallel to the wall. However, in a square duct, due to the inhomogeneous nature of the cross-sectional plane, the deposition velocities will vary over the duct walls. Two-way coupling effects and interparticle collisions are not considered in this section.

Results have been presented for ten values of τ_p^+, corresponding to two values of particle to fluid density ratio (ρ_p/ρ_f = 1000 and 8900) and five particle diameters for each density ratio. The various particle parameters considered in this section correspond to

simulations 1-10 in Table 1. In this paper, results will focus on ρ_p/ρ_f = 1000 for brevity. Figure 3 presents the wall-normal deposition velocities, as a function of deposition location, for the various τ_p^+ corresponding to ρ_p/ρ_f = 1000. Here, we see several interesting trends. First, as the Stokes number is increased from 0.072 to 1.8, the wall normal deposition velocity does not change significantly. However, further increase in τ_p^+ from 1.8 to 28.8 leads to a substantial increase in the wall-normal deposition velocity across the duct width. We see the lowest deposition velocity at the corners of the duct (deposition location = 0 and 1 in Fig. 3), and it increases progressively as we move away from the corners. The term "deposition location" represents the corresponding location on all four walls due to the 90° rotational symmetry about the duct axis. For τ_p^+ = 28.8, we also see secondary peaks in the deposition velocity at roughly 10% to 15% of the duct width from the corners. For all particle response times, we see the maximum deposition velocity at the center of the duct wall. This is due to the relatively large wall-normal gradients in the mean streamwise velocity at this location compared to the corners. This causes a larger lift force (directed towards the wall) and thus, an increased wall-normal deposition velocity.

Streamwise Deposition Velocity. Figure 4 shows that the less inertial particles deposit on the wall with lower streamwise velocities. This is because they respond better to fluid deceleration than the more inertial particles as we approach the wall. In Fig. 4, for a higher τ_p^+ = 28.8, we see that the particles tend to noticeably retain streamwise momentum after passing through the near-wall shear layer. Further, the non-uniform profiles demonstrate the effect of secondary flows.

Deposition Location. The particle deposition location is not an issue of concern for pipes and channels due to the homogeneous nature of the two directions parallel to the walls in these geometries. For a square duct, due to the additional inhomogeneous wall-normal direction, the deposition pattern is more complex. By examining the PDFs of the deposition location for τ_p^+ corresponding to ρ_p/ρ_f = 1000, shown in Fig. 5, we can identify several trends. First, deposition is always seen to be more likely near the center of the duct wall for all particle Stokes numbers examined. For the particles with τ_p^+ = 0.072 and 0.45, we see a very small fraction of particles depositing near the duct corners. As τ_p^+ is increased, deposition near the corners is higher and the particles tend to deposit more uniformly across the duct width. The wavy nature of the deposition location for higher τ_p^+ is supported by similar trends in the wall-normal deposition velocity.

Deposition Rates. Deposition rates are important in applications such as droplet impingement on a heat exchanger surface, dust deposition on surfaces in clean rooms, etc. Deposition rates will be higher for a square duct than for channel flow. This is because of the secondary flows that are more likely to transport particles to a wall.

The particle deposition rate, V_d, can be expressed as the following:

$$V_d = \frac{N_{dt}/A/t}{N/V} \qquad (1)$$

where N_{dt} is the number of deposited particles during time t, A is the area of deposition, N is the number of particles at the beginning of the deposition sampling time, and V is the volume of the domain. In Fig. 6, we compare the deposition rates, normalized by the average friction velocity, with the empirical correlations developed by McCoy and Hanratty(1977) for pipe flow. The trends are similar to those seen in pipe flow. For the τ_p^+ = 0.072 particles, the deposition rates in a square duct are seen to be up to two orders of magnitude higher than those in a pipe flow. However, for large particles, the correlation of McCoy and Hanratty (1977) agrees well with the square duct deposition rates.

Two-way Coupling and Particle Collisions

Higher volume fractions ($\phi_v = 10^{-3}$). To better understand the effects of particle feedback and collisions, we increase the volume fraction to a level where they are likely to be dominant. Therefore, one set of simulations with both two-way and four-way coupling was done for τ_p^+ = 256.32 with an initial volume fraction of 10^{-3}, which corresponds to 1.5 million particles. In this set of simulations, any significant difference between the two-way and four-way coupling results can be attributed to particle-particle collisions.

The wall-normal deposition velocity is shown in Fig. 7. Previous one-way and four-way coupled results with 100,000 initial particles ($\phi_v = 6.67\times10^{-5}$) are included for comparison. When the volume fraction is increased to 10^{-3} and only two-way coupling is considered, we see slightly higher wall-normal deposition velocities when compared to results at $\phi_v = 6.67\times10^{-5}$. This indicates that the particle feedback effect leads to a marginal increase in wall-normal deposition velocities. However, when four-way coupling at $\phi_v = 10^{-3}$ is examined, we see striking differences in the results. It is observed that the maximum wall-normal deposition velocity now occurs near the corners. The deposition velocity is increased by a factor greater than two due to collisions. This clearly indicates that the inclusion of particle-particle collisions can significantly alter the results of wall-normal deposition velocities at relatively high volume fractions.

The streamwise deposition velocity is shown in Fig. 8. With two-way coupling, the increase in volume fraction is clearly seen to decrease the streamwise deposition velocities. For $\phi_v = 10^{-3}$, inclusion of particle collisions is seen to decrease the deposition

velocity even further. Higher volume fractions are also seen to increase the non-uniformity across the duct walls for the streamwise deposition velocities. The deposition location is not significantly altered by collisions and therefore not shown.

The deposition rates for $\phi_v = 10^{-3}$, normalized by the average friction velocity, are also plotted in Fig. 6 along with the low volume fraction results. Again, we see that two-way and four-way coupling act to enhance the deposition rates.

CONCLUSIONS

The deposition of heavy solid particles in a fully developed turbulent square duct flow was studied using large eddy simulations. Ten particle Stokes numbers were studied. Two particle number densities were examined, corresponding to 10^5 and 1.5×10^6 particles initially in the domain. In addition to one-way coupling, two-way, and four-way coupling effects were also considered.

For one-way coupling, the maximum wall-normal deposition velocity occurs near the center of the duct wall. However, inclusion of particle-particle collisions results in the maximum wall-normal deposition velocity to occur near the corners. The streamwise deposition velocity also increases with particle response time. Two-way coupling and collision effects decrease the streamwise deposition velocity.

Two-way coupling effects tend to cause an augmentation of the wavy deposition pattern. Collisions do not alter the pattern of deposition locations significantly even for volume fractions up to 10^{-3}. At low volume fractions, inclusion of two-way coupling and particle collisions did not significantly alter the deposition trends.

Deposition rates are computed and compared to pipe flow experimental data. Large particles are seen to more closely match the pipe flow data. Two-way and four-way coupling enhance the deposition rates.

ACKNOWLDEGEMENTS

The financial support of the Air Conditioning and Refrigeration Center at the University of Illinois at Urbana-Champaign and the Center for Simulation of Advanced Rockets at the University of Illinois, which is funded by the US Department of Energy through the University of California under Subcontract number B341494, is gratefully acknowledged.

REFERENCES

Chen, M., Kontomaris, K., and McLaughlin, J. B., 1998, "Direct Numerical Simulation of Droplet Collisions in a Turbulent Channel Flow. Part I: Collision Algorithm," Int. J. Multiphase Flow, Vol. 24, pp. 1079-1103.

Fessler, J. R., Kulick, J. D., and Eaton, J. K., 1994, "Preferential Concentration of Heavy Particles in a Turbulent Channel Flow," Phys. Fluids, Vol. 6(11), pp. 3742-3749.

Gavrilakis, S., 1992, "Numerical Simulation of Low-Reynolds-number Turbulent Flow Through a Straight Square Duct," J. Fluid Mech. Vol. 244, pp. 101-129.

Kajishima, T., and Miyake, Y., 1992, "A Discussion on Eddy Viscosity Models on the Basis of the Large Eddy Simulation of Turbulent Flow in a Square Duct," Computers Fluids, Vol. 21(2), pp. 151-161.

Kim, W. W., and Menon, S., 1997, "Application of the Localized Dynamic Subgrid-Scale Model to Turbulent Wall-Bounded Flows," AIAA 97-0210.

Madabhushi, R. K., and Vanka, S. P., 1991, "Large Eddy Simulation of Turbulence-Driven Secondary Flow in a Square Duct," Phys. Fluids, Vol. 3(11), pp. 2734-2745.

Madabhushi, R. K., 1993, "Direct and Large Eddy Simulation of Turbulent Flow in a Square Duct," Thesis, Dept. of Mech. Eng., Univ. of Illinois at Urbana-Champaign.

McCoy, D. D., and Hanratty, T. J., 1977, "Rate of Deposition of Droplets in Annular Two-Phase Flow," Int. J. Multiphase Flow, Vol. 3, pp. 319-331.

Squires, K. D., and Eaton, J. K., 1991, "Preferential Concentration of Particles By Turbulence," Phys. Fluids, Vol. 3(5), pp. 1169-1178.

Uijttewaal, W. S. J., and Oliemans, R. V. A., 1996, "Particle Dispersion and Deposition in Direct Numerical and Large Eddy Simulations of Vertical Pipe Flows," Phys. Fluids, Vol. 8(10), pp. 2590-2604.

Wang, Q., and Squires, K. D., 1996, "Large Eddy Simulation of Particle Deposition in a Vertical Turbulent Channel Flow," Int. J. Multiphase Flow, Vol. 22(4), pp. 667-683.

Zhang, H., and Ahmadi, G., 2000, "Aerosol Particle Transport and Deposition in Vertical and Horizontal Turbulent Duct Flow," J. Fluid Mech.,Vol. 406, pp. 55-80.

Table 1: Overview of the Simulations

Simulation	ρ_p/ρ_f	d_p/δ	τ_p^+	ϕ_v	Coupling
1	1000	0.0001	0.072	8.33×10^{-9}	One-way
2	1000	0.00025	0.45	1.30×10^{-7}	One-way
3	1000	0.0005	1.8	1.04×10^{-6}	One-way
4	1000	0.001	7.2	8.33×10^{-6}	One-way
5	1000	0.002	28.8	6.67×10^{-5}	One-way
6	8900	0.0001	0.6408	8.33×10^{-9}	One-way
7	8900	0.00025	4.005	1.30×10^{-7}	One-way
8	8900	0.0005	16.02	1.04×10^{-6}	One-way
9	8900	0.001	64.08	8.33×10^{-6}	One-way
10	8900	0.002	256.32	6.67×10^{-5}	One-way
11	1000	0.0005	1.8	1.04×10^{-6}	Four-way
12	1000	0.002	28.8	6.67×10^{-5}	Four-way
13	8900	0.002	256.32	6.67×10^{-5}	Four-way
14	8900	0.002	256.32	10^{-3}	Two-way
15	8900	0.002	256.32	10^{-3}	Four-way

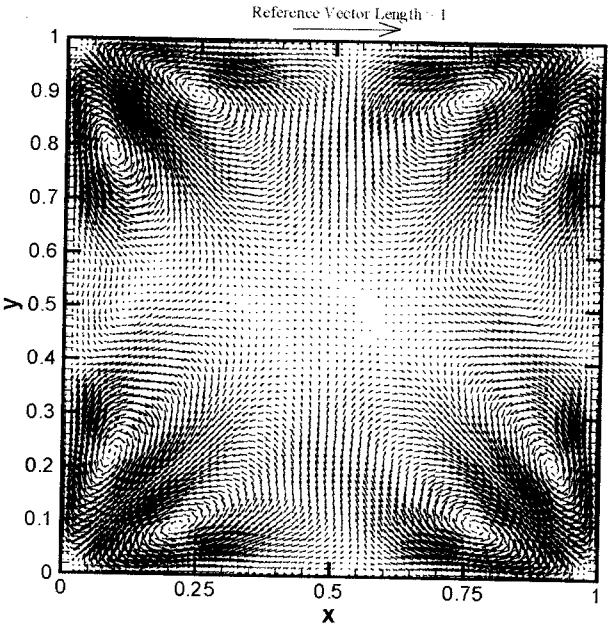

Figure 1: Mean Secondary Flows in a Square Duct

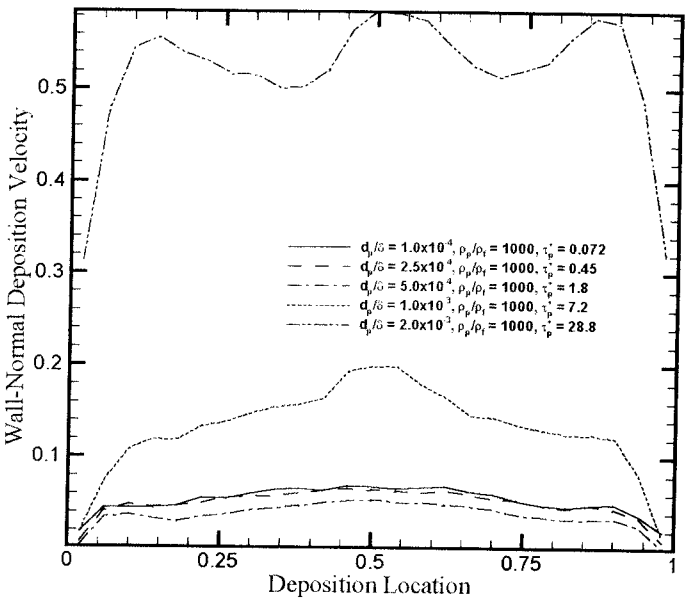

Figure 3: Wall-Normal Deposition Velocity, $\rho_p/\rho_f =$ 1000, One-way Coupling

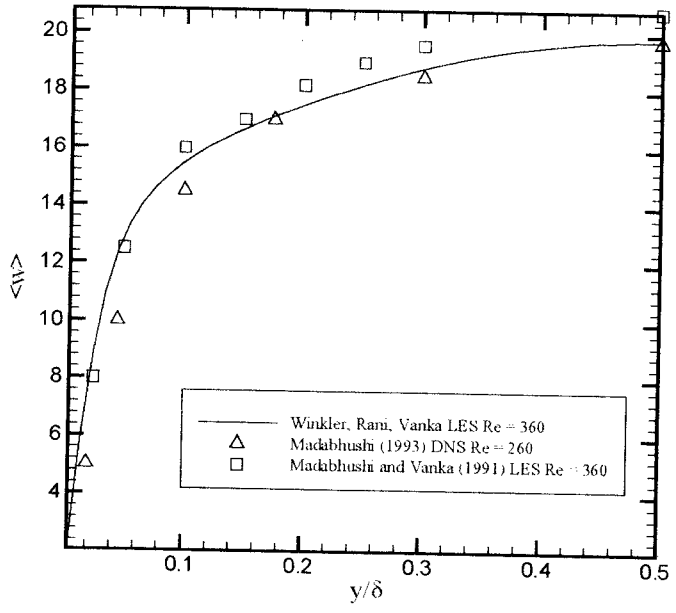

Winkler, Rani, Vanka LES Re = 360
Madabhushi (1993) DNS Re = 260
Madabhushi and Vanka (1991) LES Re = 360

y/δ

Figure 2: Comparison of Mean Streamwise Velocity at x = 0.5

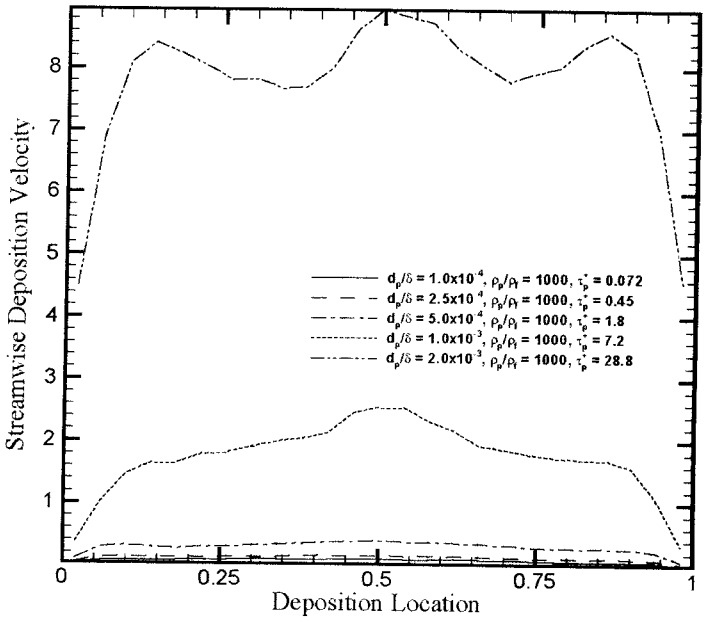

Figure 4: Streamwise Deposition Velocity, $\rho_p/\rho_f =$ 1000, One-way Coupling

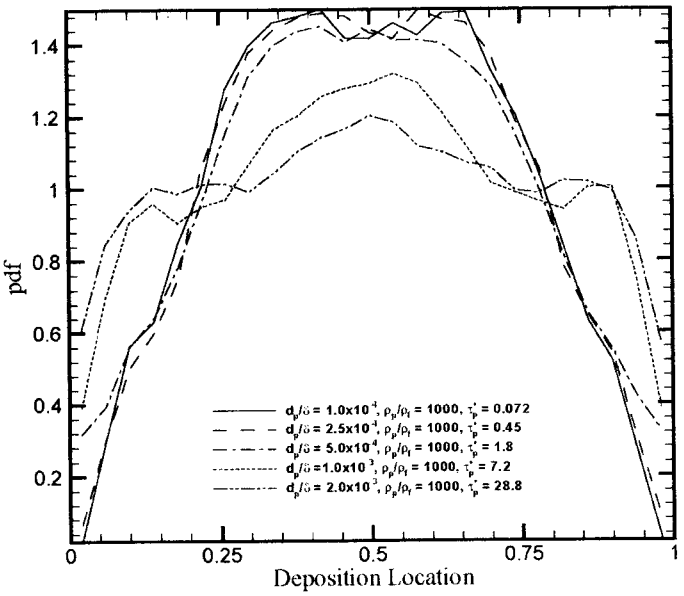

Figure 5: PDFs of Deposition Location, $\rho_p/\rho_f = 1000$, One-way Coupling

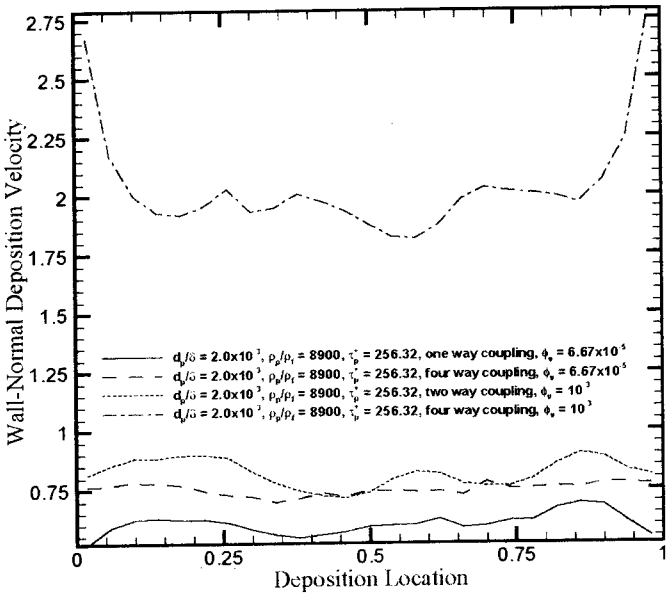

Figure 7: Wall-Normal Deposition Velocity, Two-way and Four-way Coupling, Volume Fraction = 10^{-3}

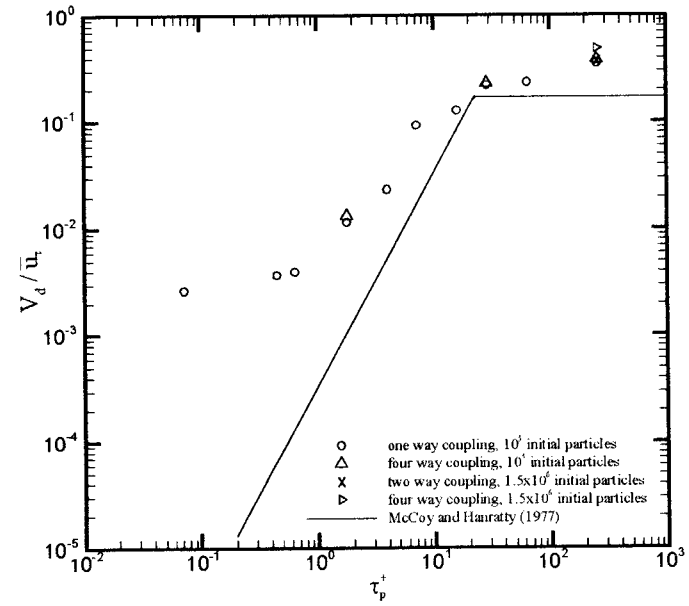

Figure 6: Deposition Rates Compared with Experimental Pipe Flow Data

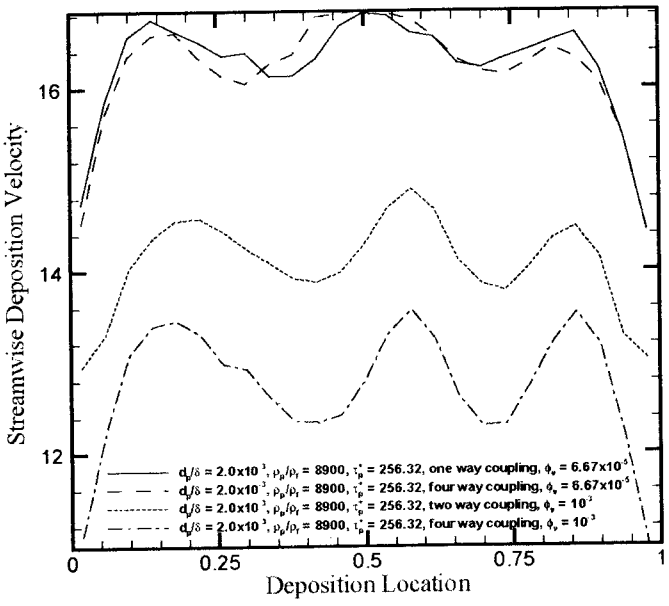

Figure 8: Streamwise Deposition Velocity, Two-way and Four-way Coupling, Volume Fraction = 10^{-3}